ILASS Americas 20th Annual Conference on Liquid Atomization and Spray Systems, Chicago, IL, May 2007

Modeling Volumetric Coupling of the Dispersed Phase using the Eulerian-Lagrangian Approach

Ehsan Shams*and Sourabh V. Apte
School of Mechanical, Manufacturing and Industrial Engineering
Oregon State University
204 Rogers Hall, Corvallis, OR 97331

Abstract

The Eulerian-Lagrangian approach is commonly used in modeling two-phase flows wherein liquid droplets, solid particles, or bubbles are dispersed in a continuum fluid of a different phase. Typically, the motion of the dispersed phase is modeled by assuming spherical, point-particles with models for added mass effects, drag, and lift forces. The effect of the dispersed phase on the fluid flow is modeled using reaction forces in the fluid momentum equation. Such an approach is valid for dilute regions of the dispersed phase. For dense regions, however, the point-particle approach does not capture the interactions between the fluid and the dispersed phase accurately. In this work, the fluid volume displaced by the dispersed phase is taken into account to model the dense regions. The motion of the dispersed phase results in local, spatio-temporal variations of the volume fraction fields. The resultant divergence in the fluid velocity acts as a source or sink displacing the flow due to dispersed phase and is termed as volumetric coupling. The size of the dispersed phase is assumed smaller than the grid resolution and for the continuum phase. The variable–density, low–Mach number equations based on mixture theory are solved using a co–located, finite volume scheme. The interphase momentum exchange due to drag forces is treated implicitly to provide robustness in the dense regions. The volumetric coupling approach is first validated with analytical studies for flow induced by oscillating bubbles and gravitational settling of particles. Simulations of Rayleigh-Taylor instability, particle-laden jet impingement on a flat plate, and particle-laden jet in a cross are performed to test the robustness of the scheme.

*Corresponding Author: shamssoe@engr.orst.edu

Introduction

Majority of spray systems in propulsion applications involve complex geometries and highly unsteady, turbulent flows near the injector. The numerical models for spray calculations should be able to accurately represent droplet deformation, breakup, collision/coalescence, and dispersion due to turbulence. In the traditional approach for spray computation, the Eulerian equations for gaseous phase are solved along with a Lagrangian model for particle transport with two-way coupling of mass, momentum, and energy exchange between the two phases [1]. Typically simulations of spray systems use DNS, LES or RANS for the carrier phase whereas the motion of the dispersed phase is modeled. The 'point-particle' (PP) assumption is commonly employed where forces on the dispersed phase are computed through model coefficients. The effect of the particles[1] on the carrier phase is represented by a force applied at the *centroid* of the particle. The disperse phase equations are typically solved in a Lagrangian frame by tracking a few set of computational particles or parcels [2] with models for droplet breakup, collision/coalescence, evaporation, dispersion, and deformation. Fully resolved simulations involving comprehensive modeling of interfacial dynamics are being developed [3, 4], however, are computationally expensive.

Several simulations of particle-laden flows have been performed with the carrier fluid simulated using direct numerical simulation ([5, 6],[7],[8]), large-eddy simulation ([9, 10, 11, 12]), or Reynolds-averaged Navier Stokes equations [13], where the dispersed phase is assumed subgrid (so $d_p < L_K$, the Kolmogorov length scale, for DNS whereas $d_p < \Delta$, the grid size, in LES or RANS). However, modeling the dispersed phase using point-particle approach does not always provide the correct results. For moderate loadings and wall-bounded flows [11] have shown that the point-particle approximation fails to predict the turbulence modulation compared to experimental values. In addition, if the particle size is comparable to the Kolmogorov scale (for DNS) or the grid size (for LES/RANS), simple drag/lift laws typically employed in PP do not capture the unsteady wake effects commonly observed in full DNS studies ([14, 15]). These effects become even more pronounced in dense particulate regions. In many practical applications, the local particle size and concentrations may vary substantially. In liquid atomization process, *e.g.*, the droplet sizes may range from 1 mm to 1 μm with dense regions near the injector nozzle. The point-particle assumption is invalid under these conditions.

In the present work, we extend the point-particle approach by accounting for the volumetric displacements of the carried phase due to the motion of particles or droplets. The disperse phase also affects the carrier phase through mass, momentum, and energy coupling. The combined effect is termed as 'volumetric coupling'. This approach is based on the the original formulation by Duckowicz [1] and later modified by Joseph & Lundgren [16]. The approach is derived based on mixture theory that account for the droplet (or particle) volume fraction in a given computational cell. This effect is important in dense spray regimes, however, are typically ignored in the context of LES or DNS simulations [17, 12]. A similar formulation has been applied to bubbly flows at low bubble concentrations (up to 0.02) to investigate the effect of bubbles on drag reduction in turbulent flows [8, 18]. Several studies on laminar dense granular flows [19, 20, 21] also use this approach. Recently, Apte *etal.* [22] have shown the effect of volumetric displacements on the carrier fluid in dense particle-laden flows. They compared the solutions for the carrier phase and the particle dispersion obtained from the point-particle assumption and accounting for volumetric displacements to show large differences. If the volume displaced by the disperse phase is taken into account, thte velocity field is no longer divergence free in the regions of variations in volume fractions. This has a direct effect on the pressure Poisson equation, altering the pressure field through a local source term. These effects may become important in dense regions of spray system.

However, computing dense spray systems by accounting for volume displacements due to droplet motion could be numerically challenging. The temporal and spatial variations in fluid volume fractions could be locally large and make the computation numerically unstable. This is specifically true if the interphase coupling of mass, momentum, and energy is treated explicitly. In the present work, we focus on non-reacting flows and only momentum exchange between the two-phases is considered. A numerical approach based on co-located grid finite-volume method is developed with part of the momentum exchange terms treated implicitly. The approach is similar to the fractional step algorithms for particle-in cell methods on staggered grids [19, 21, 20]. Implementation in co-located finite-volume formulation is discussed and is applicable to unstructured grids.

[1] In this paper, particle may mean solid particle, liquid droplets, or bubbles depending upon the case being studied.

Governing Equations

The formulation described below consists of the Eulerian fluid and Lagrangian particle equations, and accounts for the displacement of the fluid by the particles as well as the momentum exchange between them ([16]). An Eulerian-Lagrangian framework is used to solve the coupled two-phase flow equations. The disperse phase equations are solved in a Lagrangian frame with models for for drag, buoyancy, and inter-particle collision forces.

Continuum-phase equations

In the present formulation, both continuity and momentum equations account for the local concentration of particles in the continuum phase. The fluid mass for unit volume satisfies a continuity equation,

$$\frac{\partial}{\partial t}\left(\rho_f \Theta_f\right) + \bigtriangledown \cdot \left(\rho_f \Theta_f \mathbf{u}_f\right) = 0 \tag{1}$$

where ρ_f, Θ_f, and $\mathbf{u}_f$ are density, concentration, and velocity of the fluid phase respectively. Local spatio-temporal variations of particle concentration, generate a non-divergence free velocity field in the flow. The non-zero velocity divergence can be shown by rearranging the equation 1.

$$\nabla \cdot \mathbf{u}_f = -\frac{1}{\Theta_f}\frac{D\Theta_f}{Dt} \tag{2}$$

where $\frac{D}{Dt}$ is the material derivative with respect to fluid velocity.

Fluid concentration is calculated as $\Theta_f = 1 - \Theta_p$, where Θ_p is particle concentration. Lagrangian quantities, such as particle concentration, are interpolated to the Eulerian control volumes effectively, using the following interpolation function,

$$\Theta_p\left(\mathbf{x}_{cv}\right) = \sum_{p=1}^{N_p} V_p \mathcal{G}_\Delta\left(\mathbf{x}_{cv}, \mathbf{x}_p\right) \tag{3}$$

where $\mathbf{x}_{cv}$ and $\mathbf{x}_p$ are control volume and particle positions, respectively, V_p is the particle volume, $\mathcal{G}_\Delta$ is the interpolation function, N_p is the total number of particles, and the summation is over all particles.

Momentum conservation is also satisfied by solving

$$\begin{aligned}\frac{\partial}{\partial t}\left(\rho_f \Theta_f \mathbf{u}_f\right) + \nabla \cdot \left(\rho_f \Theta_f \mathbf{u}_f \mathbf{u}_f\right) = \\ -\nabla\left(\Theta_f p\right) + \nabla \cdot \left(\mu_f \mathbf{D}_c\right) + \mathbf{F}\end{aligned} \tag{4}$$

where p is dynamic pressure, μ_f is the fluid viscosity, $\mathbf{D}_c = \nabla \mathbf{u}_c + \nabla \mathbf{u}_c^{\mathrm{T}}$ is the deformation tensor of the mixture, $\mathbf{u}_c = \Theta_f \mathbf{u}_f + \Theta_p \mathbf{u}_s$ is the composite velocity of mixture, and $\mathbf{F}$ is the reaction force from the particle phase on the fluid phase per unit mass of fluid. Average particle velocity in control volume, $\mathbf{u}_s$ is calculated using the interpolation function

$$\Theta_p \mathbf{u}_s = \sum_{p=1}^{N_p} V_p \mathcal{G}_\Delta\left(\mathbf{x}_{cv}, \mathbf{x}_p\right) \mathbf{u}_p \tag{5}$$

where $\mathbf{u}_p$ is the particle velocity.

Particle-phase equations

Position and velocity of particles are calculated by solving the ordinary differential equations of motion in Lagrangian form,

$$\frac{\mathrm{d}}{\mathrm{dt}}\left(\mathbf{x}_p\right) = \mathbf{u}_p \tag{6}$$

$$m_p \frac{\mathrm{d}}{\mathrm{dt}}\left(\mathbf{u}_p\right) = \sum \mathbf{F}_p \tag{7}$$

where $\mathbf{x}_p$ and $\mathbf{u}_p$ are particle position and velocity, m_p is the mass of particle, and $\sum \mathbf{F}_p = m_p \mathbf{A}_p$ is the total force acting on particle, and $\mathbf{A}_p$ is the particle acceleration. In this study, only the effect of drag, gravitational force, and the inter-particle collisions are considered. For high density ratios between the disperse phase and the carrier phase (typical of spray systems), the lift forces, added mass, and history forces are much smaller than the drag force and are neglected in this study. The total particle acceleration is given as:

$$\mathbf{A}_p = \underbrace{D_p\left(\mathbf{u}_{f,p} - \mathbf{u}_p\right)}_{\mathbf{A}_{drag}} + \underbrace{\left(1 - \frac{\rho_f}{\rho_p}\right)\mathbf{g}}_{\mathbf{A}_{gravity}} + \mathbf{A}_{cp} \tag{8}$$

where $\mathbf{u}_{f,p}$ is the fluid velocity at the particle position and $\mathbf{A}_{cp}$ is the particle acceleration due to inter-particle collisions. The inter-particle force is modeled by the discrete-element method of Cundall & Strack as described by [20]. The drag force is caused by the motion of a particle through the gas. In the drag model D_p is defined as

$$D_p = \frac{3}{8} C_d \frac{\rho_f}{\rho_p} \frac{\mid \mathbf{u}_{f,p} - \mathbf{u}_p \mid}{r_p} \tag{9}$$

where C_d is given by [23]

$$\begin{aligned} C_d = \frac{24}{\mathrm{Re}_p}\left(1 + a\mathrm{Re}_p^b\right)\Theta_f^{-2.65}, \qquad & \mathrm{Re}_p < 1000 \\ C_d = 0.44\Theta_f^{-2.65}, \qquad & \mathrm{Re}_p > 1000 \end{aligned} \tag{10}$$

where the particle Reynolds number is defined as

$$\mathrm{Re}_p = \frac{2\rho_f \Theta_f \mid \mathbf{u}_{f,p} - \mathbf{u}_p \mid r_p}{\mu_f} \tag{11}$$

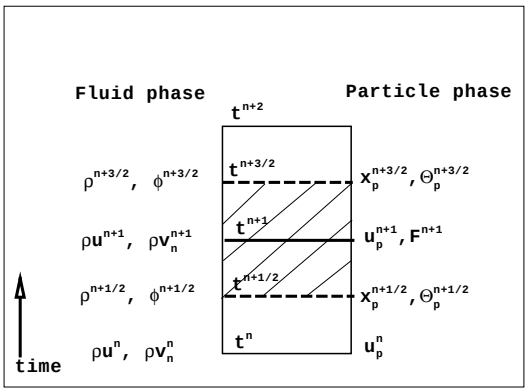

Figure 1: Staggering of variables of each phase

and

$$r_p = \left(\frac{3V_p}{4\pi}\right)^{1/3} \tag{12}$$

is the particle radius.

Numerical Scheme

The numerical scheme is based on a co-located grid, fractional step finite-volume approach. The fluid flow is solved on a structured grid (generalization to unstructured grids are feasible [24] For the present volumetric coupling, fluid flow equations become similar to the variable-density low-Mach number formulation [12]. The numerical scheme presented here have the following important features: (i) a time-staggered, co-located grid based fractional step scheme, (ii) low-Mach number variable density flow solver, (iii) accounting for volume displacement effect of the Lagrangian particles on the fluid flow, (iv) implicit coupling of particle-fluid momentum exchange in the numerical solution, and (v) using Gaussian kernel for interpolation of Lagrangian quantities to the Eulerian grid.

In many particle-laden flow regimes, where the particle loading is high, the effect of particle reaction force on the flow is important. In regions of very dense loading, the momentum coupling force could be very large, and its explicit treatment affects the robustness of the flow solver. An implicit treatment of the reaction force is thus necessary. In simulations considered here only the inter-phase drag force is treated implicitly. Numerical solution of the governing equations of continuum phase and particle phase are staggered in time to maintain time-centered, second-order advection of the particle and fluid equations. Figure 1 shows staggering of variables of each phase in time. Denoting the time level by a superscript index, the velocities are located at time level t^n and t^{n+1}, and pressure, density, viscosity, the signed distance function, and the color function at time levels $t^{n-1/2}$ and $t^{n+1/2}$. Particle velocity ($\mathbf{u}_p$) and inter-phase coupling force ($\mathbf{F}$) are treated at times n and $n+1$, whereas particle position ($\mathbf{x}_p$) and concentration (Θ_p) are calculated at times $n+1/2$ and $n+3/2$.

The continuity equation of the fluid phase is discretized as

$$\frac{\rho^{n+3/2}-\rho^{n+1/2}}{\Delta t} + \frac{1}{V_{cv}} \sum_{\text{faces of cv}} (g_N)^{n+1} A_{\text{face}} = 0 \tag{13}$$

where N stands for face-normal, face for face of a control volume (cv), and $g_N^{n+1} = \rho^{n+1} u_N^{n+1}$ and $\rho = \rho_f \Theta_f$.

Particle velocity in the implicit formulation is written as

$$\frac{\mathbf{u}_p^{n+1}-\mathbf{u}_p^n}{\Delta t} = -\left(\frac{\mathbf{u}_p^{n+1}-\mathbf{u}_{f,p}^{n+1}}{\tau_r}\right) + \mathbf{A}_{cp}^{n+1} + \left(1-\frac{\rho_f}{\rho_p}\right)\mathbf{g} \tag{14}$$

where $\mathbf{u}_{f,p}^{n+1}$ is the interpolated velocity of fluid phase at time $n+1$ to the particle location. From the above formulation, one can obtain

$$\mathbf{u}_p^{n+1} = \frac{1}{1+\frac{\Delta t}{\tau_r}}\left[\mathbf{u}_p^n + \left(\frac{\Delta t}{\tau_r}\right)\mathbf{u}_{f,p}^{n+1} + \Delta t \mathbf{A}_{cp}^{n+1} + \Delta t\left(1-\frac{\rho_f}{\rho_p}\right)\mathbf{g}\right] \tag{15}$$

Note that for an isolated particle, in the absence of any external forces, for an extremely heavy particle $\tau_r \to \infty$ and we get $\mathbf{u}_p^{n+1} \to \mathbf{u}_p^n$. Whereas for a massless particle, $\tau_r \to 0$ and we obtain $\mathbf{u}_p^{n+1} \to \mathbf{u}_{f,p}^{n+1}$. The numerical algorithm consists of the following steps:

Step 1

First obtain drag and collision forces at time n then update the particle position explicitly:

$$\begin{aligned}\mathbf{x}_p^* &= \mathbf{x}_p^{n+1/2} + \Delta t \mathbf{u}_p^{n+1} \\ &= \mathbf{x}_p^{n+1/2} + \Delta t\left(\mathbf{u}_p^n + \Delta t \mathbf{A}_p^n\right)\end{aligned}$$

where $\mathbf{A}_p$ is the total particle acceleration from 8. Based on the new particle positions, the inter-particle acceleration due to collision is computed at the new position. Then set $\mathbf{A}_{cp}^{n+1} = (\mathbf{A}_{cp}^{n+1/2} + \mathbf{A}_{cp}^{n+3/2})/2$.

Step 2

Compute the particle and fluid volume fractions at $x^{n+3/2}$ by interpolating from the Lagrangian particle positions to the Eulerian grid cv centers. Set

predictors for fluid phase density and face-normal velocity (u_N), then advance scalars.

$$\rho^* = \rho^{n+3/2}\Theta_f^{n+3/2}$$
$$u_N^* = u_N^{n+1}$$

Step 3

Advance the gas-phase momentum equation using the fractional step method [25]

$$\frac{\rho^* {u_i}^*}{\Delta t} + \frac{1}{2V}\sum_{\text{faces of cv}} \left[u^n_{i,\text{face}} + u^*_{i,\text{face}}\right] g_N^{n+1/2} A_{\text{face}} = \frac{\rho^n {u_i}^n}{\Delta t} - \frac{\partial p^n}{\partial x_i} + \frac{1}{2V}\sum_{\text{faces of cv}} \mu_{\text{face}} \left(\frac{\partial u^*_{i,\text{face}}}{\partial x_j} + \frac{\partial u^n_{i,\text{face}}}{\partial x_j}\right) A_{\text{face}} - \frac{2}{3}\frac{\partial}{\partial x_j}\left(\mu \frac{\partial u_k^n}{\partial x_k}\delta_{ij}\right) + F_i^*$$

where $g_N^{n+1/2} = (g_N^* + g_N^n)/2$ and $g_N^* = \rho^* u_N^*$. Using the particle momentum equation (14), gives the implicit formula for the fluid phase advancement. In a fractional step scheme, the reaction force $F_i^*$is written as

$$F_i^* = -\mathcal{T}\left(u_i^*\right) + \mathcal{T}\left(u_{p,i}^n\right) + \Delta t \mathcal{T}\left(A_{cp,i}^{n+1} + A_{gravity,i}^{n+1}\right)$$

where the operator $\mathcal{T}$ is

$$\mathcal{T} = \sum_p \left[\mathcal{G}_\Delta(\mathbf{x}_p^{n+1}) \frac{m_p/\tau_r}{1 + \frac{\Delta t}{\tau_r}}\right]. \tag{16}$$

The first term on the right hand side of F_i^* is an implicit in terms of u_i^*.

Step 4

Remove the old pressure gradient to obtain

$$\widehat{g_i} = g_i^* + \Delta t \frac{\partial p}{\partial x_i}^n \tag{17}$$

Step 5

Interpolate the velocity field to the control volume faces and solve the Poisson's equations is solved for pressure,

$$\bigtriangledown^2(p\Delta t) = \frac{1}{V}\sum_{\text{faces of cv}} \widehat{g_{i,\text{face}}} A_{\text{face}} + \frac{\rho^{n+3/2} - \rho^{n+1/2}}{\Delta t} \tag{18}$$

Step 6

Compute the new face-velocities satisfying continuity equation 13

$$\frac{g_N^{n+1} - \widehat{g_N}}{\Delta t} = -\frac{\partial p}{\partial N}^{n+1} \tag{19}$$

Step 7

Reconstruct the pressure gradient,

$$\frac{\partial p^{n+1}}{\partial x_i} = \overline{\left(\frac{\partial p^{n+1}}{\partial N}\right)}^{LS} \tag{20}$$

where $\overline{(\ )}^{LS}$ stands for least-squares interpolation used by [24]. Now update the *cv* center velocities

$$\frac{g_i^{n+1,*} - \widehat{g_i}}{\Delta t} = -\frac{\partial p^{n+1}}{\partial x_i} \tag{21}$$

Step 8

Now advance the particle velocity field using equation 14 and the interpolated carrier-phase velocity field $\mathbf{u}_f^{n+1,*} = g_i^{n+1,*}/\rho^{n+1}$.

$$\frac{m_p\left(\mathbf{u}_p^{n+1} - \mathbf{u}_p^n\right)}{dt} = \mathbf{F}_p^{n+1} = m_p \mathbf{A}_p^{n+1} = m_p\left(\frac{\mathbf{u}_{f,p}^{n+1,*} - \mathbf{u}_p^{n+1}}{\tau_r} + \mathbf{A}_{cp}^{n+1} + \left(1 - \frac{\rho_g}{\rho_p}\right)\mathbf{g}\right)$$

Step 9

In general (on non-uniform grids), the interpolation operator from the grid CVs to the particle location and the inverse operator (from the particle location to the grid CVs) may not commute. To obtain discrete momentum conservation between the two-phases, any residual force is applied to the carrier-phase velocity field in an explicit form,

$$\rho^{n+1} u_i^{n+1} = \rho^{n+1} u_i^{n+1,*} - \Delta t\left(\sum_p \left[u_{i,fp}^{n+1,*} \frac{\mathcal{G}_\Delta(\mathbf{x}_p^{n+1}) m_p/\tau_r}{1 + \Delta t/\tau_r}\right] - u_i^{n+1,*}\sum_p \left[\frac{\mathcal{G}_\Delta(\mathbf{x}_p^{n+1}) m_p/\tau_r}{1 + \Delta t/\tau_r}\right]\right) \tag{22}$$

The above correction is usually small and does not introduce time-step restrictions comparable to fully explicit interphase coupling.

Results

The above numerical scheme is applied to different test cases in order to evaluate its accuracy and robustness. These test cases are described below.

Oscillating bubble

First we show the importance of volumetric displacement effect on the flow filed, caused by change in local concentration of particles. The variable density formulation used in these simulations accounts

for changes in the density of mixture. This can be the result of particle accumulation/scattering in the flow field due to inter-phase momentum exchanges, or size variation in a cavitating bubble due to hydrodynamic pressure of the flow, etc. Here we set up a very simple case of imposed oscillation on the radius of a bubble which causes a potential flow filed around itself. This phenomenon can not be simulated by only inter-phase momentum coupling and here we show that only through the variations in density in momentum and continuity equation, the potential flow is expressed.

We put a single air bubble in a cube of water and impose sinusoidal perturbation on the bubble radius. Bubble radius changes in time as $R = R_0 + e\sin(\omega t)$, where R and R_0 are the instantaneous and the initial radius, respectively, e is the perturbation magnitude, ω is frequency and t is time. In this simulation, $R_0 = 0.01 \times D$, where D is the cube size, and gives overall concentration of 4×10^{-6}, $e = 0.1 \times R_0$, $\omega = 50[Hz]$. Figure 2 shows the radial distribution of hydrodynamic pressure around the bubble created by the size variation at $t^* = 0.3$ where $t^* = t/T$ and $T = 2\pi/\omega$. We compare the pressure with analytical

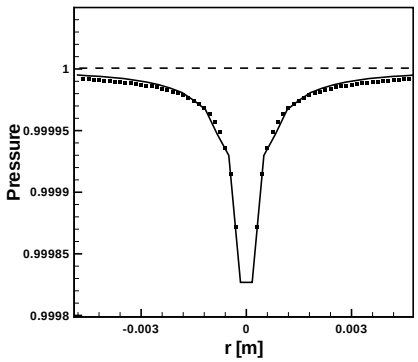

Figure 2: Pressure distribution caused by volume displacement around the bubble, from two-way coupling (dashed line), volumetric coupling (solid line), and analytical solution (dots).

solution (dots), given by [26] and result with two-way coupling and no volumetric effect (dashed line). The two-way coupling did not show any effect on the pressure, however the volumetric coupling result is in good agreement with the analytical solution.

In another similar example we consider two bubbles oscillating in tandem. Two similar bubbles are put in a box and their radius changes sinusoidally with π [rad] phase shift. All properties are similar to the case of single bubble case, except they are

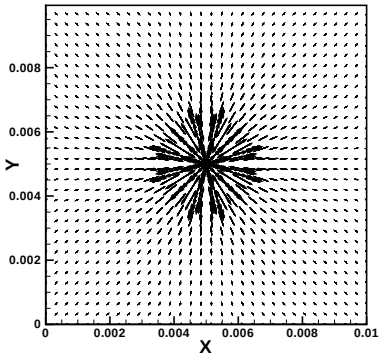

Figure 3: Velocity vectors around the bubble caused by radius variations

both located $D/6$ away from the box center. The result is a doublet-like flow which is shown in figure 4. Again in this case we did not observe any

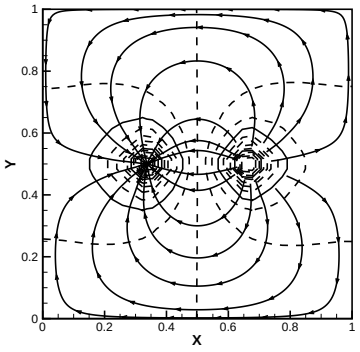

Figure 4: Doublet generated by bubbles oscillating in tandem

effect on the flow in two-way coupling results.

Gravitational Settling

We simulate sedimentation of solid particles under gravity in a rectangular box. Details of this case are given in Table 1. The initial parcel positions are generated randomly over the entire length of the box. A parcel consists of a group of particles of equal diameter which move together. These parcels are then allowed to settle through the gas-medium under gravity. The dominant forces on the particles include gravity and inter-particle/particle-wall collision. As the particles hit the bottom wall of the box, they bounce back and stop the incoming layer of particles, and finally settle to a close pack limit (~ 0.6). Figures 5(a-c) show the time evolution of

Table 1: Parameter description for gravity-dominated sedimentation.

Computational domain,	$0.2 \times 0.6 \times 0.0275$ m
Grid	$10 \times 30 \times 5$
Fluid density	1.25 kg/m^3
Particle Density	2500 kg/m^3
Number of Parcels	1000
Particles per parcel	3375
Diameter of particles	500 μm
Initial concentration	0.2

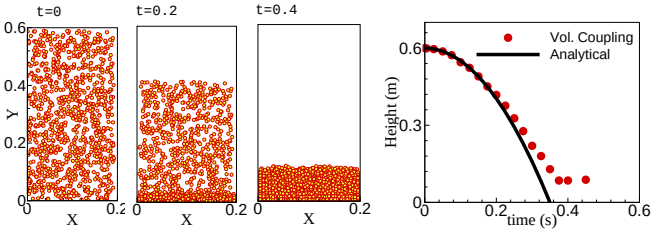

Figure 5: Temporal evolution of particle distribution during gravity-dominated sedimentation: a) $t = 0$, b) $t =$, c) $t =$, d) Height from bottom wall compared with theory ($H = H_0 - 0.5gt^2$)

particle positions in the rectangular box. The particles eventually settle down with close-packing near the bottom wall. Figure 5d shows the temporal evolution of the interface. The numerical formulation for volumetric coupling predict the interface evolution similar to the analytical estimate $h = gt^2/2$. As the particles settle, they accelerate the fluid in the upward direction, however, the effect of the drag force on the particle motion was found to be small. The volume fraction of the particles reaches the theoretical maximum (0.6 is the close pack limit) as they accumulate near the bottom wall. The numerical scheme was stable and able to handle strong variations in the volume fraction.

Rayleigh-Taylor instability

We consider the sedimentation case generating Rayleigh-Taylor instability similar to that studied by Snider [21]. A set of heavy particles are initially arranged uniformly above a light fluid and the initial concentration is approximately 0.038. The interface between the particles and the fluid is perturbed by a cosine wave initially which causes an exponential growth in the mixture. The parameters in this study are presented in table 2. The computational domain is [1 4] and the grid resolution used is 64×256. Slip wall conditions are used for the top and bottom walls and periodic conditions are used in the x direction.

Particle radius [μm]	3250
Fluid density [kg/m^3]	0.1694
Particle density [kg/m^3]	1.225
Initial particle volume fraction	3.77 $\times 10^{-2}$
Number of particles	131,000
Gravity in y direction [m/s^2]	-9.81

Table 2: Fluid and particle properties in Rayleigh-Taylor instability.

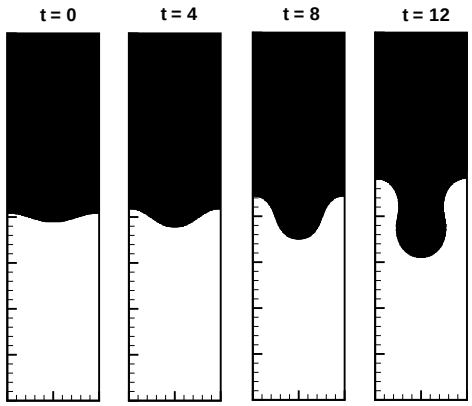

Figure shows the time evolution of the particle volume fraction. The initial perturbation grows as the particles are accelerated downward by gravity. In the central region, the falling particles push the fluid downward which rises from the edges of the computational domain pushing the particles upward in Rayleigh-Taylor instability. Particles fall at a higher rate than their terminal velocity. This is due to the effect of upward flow generated by this motion near the edges of the computational domain. The circulation caused by this motion is shown in figure 6. As presented by [21], this height (H) is a function of Atwood number, defined as $A = (\rho_p - \rho_f)/(\rho_p + \rho_f)$, gravity, and time. Initially, it grows exponentially in time until the interface deforms.

Particle-laden jet impingement

This test case is similar to that studied by Snider [21] and evaluates the robustness of the current numerical approach for dense particle systems. A jet of particles from a 1.5 cm tube is directed onto a flat plate at high velocity. Particles are fed at an initial volume fraction of 0.3 at a velocity of 25 m/s.

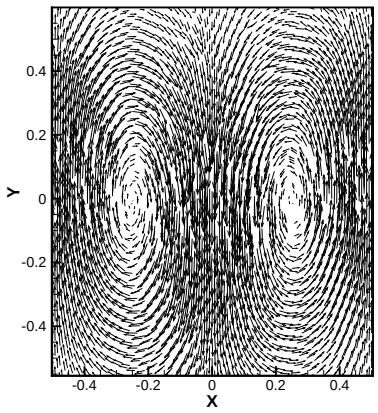

Figure 6: Circulation generated by particles

Table 3 shows the flow parameters used. At the top and bottom boundaries of the domain, no-slip conditions are applied. The left and right boundaries are considered outflow. A stable solution is obtained for large variations in the particle volume fractions in this dynamic problem. An explicit drag force resulted in blow-up of the flow solver.

Particle radius [μm]	100
Fluid density [kg/m^3]	1
Particle density [kg/m^3]	2760
Initial particle volume fraction	0.3
Gravity in y direction [m/s^2]	-9.81
Time step [s]	5×10^{-5}
Computational Domain [cm]	$27 \times 27 \times 17$
Grid	$24 \times 24 \times 14$

Table 3: Fluid and particle properties in particle-laden jet impingement case

Particle-laden jet in cross flow

Finally, we simulate the effect of particle-laden jet on a laminar channel flow. The inlet flow is a plane Poiseuille flow and the particles are injected at x = 0.01[m] away from the inlet. Table 4 shows the parameters of this simulation. Particles are added continuously in the form of a round circular jet. The maximum particle volume fraction inside the jet is approximately 0.2. Figure 8 shows the velocity vectors of the channel flow under the influence of the particle jet. The velocity vectors show a circulation region generated behind the jet. Figure 9 also shows evolution of vorticity contours due to presence of the particle jet. Both figures show that the combined ef-

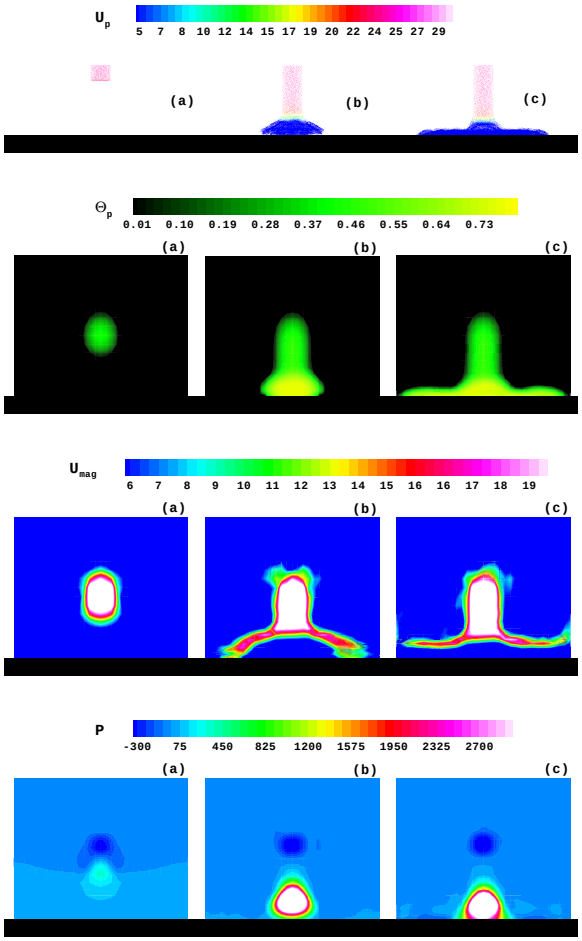

Figure 7: Time evolution of particle-laden jet impinging on a flat plate: (i) particle evolution, (ii) fluid volume fraction, (iii) fluid velocity magnitude, and (iv) pressure.

fect of upward momentum from particles to the the continuum phase and volumetric displacement effect due particles, generate a strong circulation in the flow field.

Summary and Conclusion

A numerical formulation based on time-staggered, co-located grid, finite volume approach is developed for simulation of dense particle-laden flows. The original formulation for spray systems by Duckowiz [1] was used to discretize the governing equations for a non-reacting, incompressible fluid-laden with particles on structured grids. This formulation takes into account for the fluid displaced by the particle motion ('volumetric coupling') in terms of a fluid volume fraction . In addition, the interphase momentum coupling is modeled through a re-

Channel height [m]	0.02
Channle length [m]	0.05
Maxium flow velocity at inlet [m/s]	5
Particle vertical velocity component at injection [m/s]	1.25
Fluid density [kg/m^3]	1
Particle density [kg/m^3]	1000
Particle diameter [μm]	40
Maximum particle volume fraction	0.2
Number of particles	10^6

Table 4: Simulation settings for particle jet in cross flow

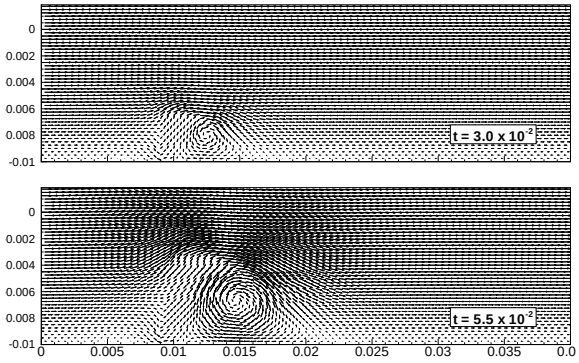

Figure 8: Velocity vectors generated by jet in cross flow at different times

action force exerted by the disperse phase on the carrier fluid. For dense regions of particle concentrations, the interphase drag force is treated implicitly in a fractional step method to improve robustness of the approach. Several test cases are considered to evaluate the accuracy and robustness of the numerical scheme for dense loadings. First, the effect of a single bubble undergoing forced periodic oscillations is computed by considering the present approach as well as the standard 'two-way' coupling based point-particle method to show large variations in the predicted flow field. The results are compared with analytical solutions to validate the numerical approach for volumetric coupling. A test case with two bubbles undergoing forced oscillations in tandem is also investigated. The doublet-like flow pattern is well predicted by the present approach. Next, standard test cases of (i) gravitational settling, (ii) Rayleigh-Talor instability, (iii) particle-laden jet impingement

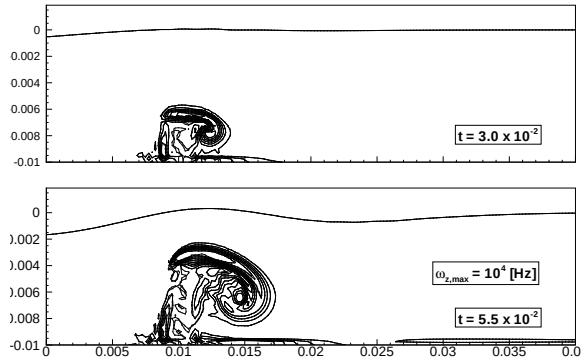

Figure 9: Vorticity contours generated by jet in cross flow at different times

on a flat plate, and (iv) particle-laden jet in a cross flow are simulated to test the robustness of the numerical scheme under dense loading. The numerical approach is fully three-dimensional and applicable to structured or unstructured grids.

The present numerical approach is capable of simulated dense regions of spray systems near the injector. Two issues that need further investigation are: (i) This approach, however, requires that the grid used for fluid flow solver be coarser than the size of the particles (or droplets). As the computational grid becomes completely occupied by the disperse phase, a continuum formulation should be used for the dispersed phase. A hybrid approach combining discrete and continuum approaches is necessary to model the different regimes of dense spray systems. (ii) Equations, closure models, and numerical techniques for volumetric coupling in the context of large-eddy simulation are needed for dense particle/droplet-laden systems. The fluid volume fraction (Θ_f) together with the fluid density ρ_f can be used to define an effective fluid density ($\rho = \rho_f \Theta_f$) and density-weighted Favre-averaging can be used to derive filtered equations for the resolved scales in LES. Models for closure of the subgrid-scale terms involving fluid volume fraction need to be developed.

References

[1] John K. Dukowicz. *Journal of Computational Physics*, 35(2):229–253, 1980.

[2] PJ O'Rourke and FV Bracco. *Proc. of the Inst. of Mech. Eng*, 9:101–106, 1980.

[3] S. Tanguy and A. Berlemont. *Int. J. Mult. Flow*, 31:1015–1035, 2005.

[4] M. Gorokhovski and M. Herrmann. *Ann. Rev. Fl. Mech.*, 40:343–366, 2008.

[5] S. Elghobashi. *Flow, Turbulence and Combustion*, 52(4):309–329, 1994.

[6] Walter C. Reade and Lance R. Collins. *Physics of Fluids*, 12(10):2530–2540, 2000.

[7] D.W.I. ROUSON and J.K. EATON. *Journal of Fluid Mechanics*, 428:149–169, 2001.

[8] JIN XU, M.R. MAXEY, and G.E.M. KARNIADAKIS. *Journal of Fluid Mechanics*, 468:271–281, 2002.

[9] Qunzhen Wang and Kyle D. Squires. *Physics of Fluids*, 8(5):1207–1223, 1996.

[10] S. V. Apte, K. Mahesh, P. Moin, and J. C. Oefelein. *International Journal of Multiphase Flow*, 29(8):1311–1331, 2003.

[11] J.C. Segura, J. K. Eaton, and J. C. Oefelein. PhD thesis, STANFORD UNIVERSITY, 2005.

[12] P. Moin and S.V. Apte. *accepted for publication in AIAA J.*, 2005.

[13] M. Sommerfeld, A. Ando, and D. Wennerberg. *ASME, Transactions, Journal of Fluids Engineering*, 114(4):648–656, 1992.

[14] T.M. Burton and J.K. Eaton. *Journal of Fluid Mechanics*, 545:67–111, 2005.

[15] P. Bagchi and S. Balachandar. *Physics of Fluids*, 15:3496–3513.

[16] DD Joseph, TS Lundgren, R. Jackson, and DA Saville. *International journal of multiphase flow*, 16(1):35–42, 1990.

[17] S. V. Apte, M. Gorokhovski, and P. Moin. *International Journal of Multiphase Flow*, 29(9):1503–1522, 2003.

[18] A. Ferrante and S. Elghobashi. *Physics of Fluids*, 15(2):315–329, 2003.

[19] MJ Andrews and PJ O'Rourke. *International Journal of Multiphase Flow*, 22(2):379–402, 1996.

[20] N. A. Patankar and D. D. Joseph. *International Journal of Multiphase Flow*, 27(10):1685–1706, 2001.

[21] D. M. Snider. *Journal of Computational Physics*, 170(2):523–549, 2001.

[22] S. V. Apte, K. Mahesh, and T. Lundgren. *International Journal of Multiphase Flow*, 34(3):260–271, 2008.

[23] D. Gidaspow. *Multiphase Flow and Fluidization: Continuum and Kinetic Theory Descriptions*. Academic Press, 1994.

[24] K. Mahesh, G. Constantinescu, and P. Moin. *Journal of Computational Physics*, 197(1):215–240, 2004.

[25] K. Mahesh, G. Constantinescu, S. Apte, G. Iaccarino, F. Ham, and P. Moin. *Journal of Applied Mechanics*, 73:374, 2006.

[26] R.L. Panton. *Incompressible Flow*. Wiley-Interscience, 2006.